arXiv:2007.01356v1 [stat.ML] 2 Jul 2020

# Decoder-free Robustness Disentanglement without (Additional) Supervision

**Yifei Wang***
Peking University
yifei_wang@pku.edu.cn

**Dan Peng**
Huawei Noah's Ark Lab
pengdancs@gmail.com

**Furui Liu**
Huawei Noah's Ark Lab
liufurui2@huawei.com

**Zhenguo Li**
Huawei Noah's Ark Lab
li.zhenguo@huawei.com

**Zhitang Chen**
Huawei Noah's Ark Lab
chenzhitang2@huawei.com

**Jiansheng Yang**
Peking University
yjs@math.pku.edu.cn

## Abstract

Adversarial Training (AT) is proposed to alleviate the adversarial vulnerability of machine learning models by extracting only robust features from the input, which, however, inevitably leads to severe accuracy reduction as it discards the non-robust yet useful features. This motivates us to preserve both robust and non-robust features and separate them with disentangled representation learning. Our proposed Adversarial Asymmetric Training (AAT) algorithm can reliably disentangle robust and non-robust representations without additional supervision on robustness. Empirical results show our method does not only successfully preserve accuracy by combining two representations, but also achieve much better disentanglement than previous work.

## 1 Introduction

A well-known obstacle of machine learning is the existence of adversarial examples. A small invisible perturbation to the input can lead to dramatic misbehavior of neural networks [26], raising huge concern about the vulnerability of machine learning. Various attack and defense algorithms have been developed ever since, like a cat and mouse game [3].

Adversarial Training [6] is proposed to train a classifier with adversarial examples and effectively makes it more robust to perturbations. Perhaps surprisingly, it is found that the robust features, i.e., image features utilized by robust classifiers, are perceptually aligned with humans [22]. On the contrary, the non-robust features from a standard classifier, are also useful for classification but look like plain noise to humans. This indicates that adversarial training is founded on a human-centric perspective [11], that it enforces neural networks to achieve the robustness defined by human recognition, i.e., robustness against perturbations, which, however, may conflict with the nature of neural networks. As a result, adversarial training of neural networks will inevitably lead to severe accuracy reduction in the classification of natural images [27].

Nevertheless, robustness is desirable in some scenarios where humans are involved in the loop. In the meantime, non-robust features also matter for accuracy, and it seems unwise to discard them as in adversarial training. As Bengio et al. [1] put it, *the most robust approach to feature learning is to disentangle as many factors as possible, discarding as little information about the data as is practical*. Motivated by this, instead of keeping either of them, we propose to map robust and non-robust features into two disentangled representations. Thus, both robust and non-robust features are not only

*Work was done during an internship at Huawei Noah's Ark Lab.

Preprint. Under review.

preserved but also well separated. Afterwards, we can obtain a robust or non-robust classifier with only one of the representations, or achieve better accuracy by combining two representations when necessary.

Learning deep representations where different semantic aspects of data are structurally disentangled is of central importance for training robust models [1, 25]. To achieve disentanglement, supervised methods require access to additional supervision, in the form of pairwise data sharing the same attributes [18], or the ground truth generative mechanism [15], etc. But those supervisions are hardly available in practice. Alternatively, some focus on disentangling latent factors purely from unsupervised data [10, 13], which, however, are challenged lately [16] as their disentanglement scores are heavily influenced by randomness, and the disentanglement shows no clear benefit for downstream tasks.

Our method has advantages over both diagrams. On the one hand, we can disentangle robust and non-robust features without additional supervision on robustness. With class-labeled data, previous work [23, 7] can only disentangle w.r.t. class itself, while ours can disentangle w.r.t. robustness, which is not directly given by data. On the other hand, the unsupervised methods mostly rely on Variational Autoencoders [14] with unstable performance [16], while our model is more efficient and effective as it is deterministic, decoder-free, and able to produce successful disentanglement with little random variability. Last but not least, our disentanglement shows clear benefits for downstream applications, such as standard and adversarial predictions, as well as adversarial detection and calibration.

But how to achieve the disentanglement remains unclear. For a natural image, its robust and non-robust features are entangled together, and we hardly know the ground truth of either of them. Ilyas et al. [11] developed an iterative optimization scheme that constructs images with only robust or non-robust features of a natural image, for which we call *pseudo-inputs*. Experiments show that they can achieve a limited degree of disentanglement, but cause even worse accuracy reduction because the generation of pseudo-inputs leads to a great loss of details in the raw images.

Our disentanglement method is based on the idea of *pseudo-pairs* instead. We notice that essentially the process of adversarial attack is about modifying the non-robust features such that they belong to a wrong class and lead to misclassification of the images. Therefore, a misclassified adversarial example is supposed to contain robust and non-robust features about different classes, and the combination of a natural and an adversarial example yields a *pseudo-pair* for robustness disentanglement. Based on this insight, we propose *Adversarial Asymmetric Training (AAT)* that assigns asymmetric labels to robust and non-robust representations, and the asymmetry disentangles them apart. Vanilla Adversarial Training extracts robust features alone and fails at preserving standard accuracy, while our AAT extracts both kinds of features with disentanglement, and makes it possible to preserve accuracy by combining two representations. Compared to the pseudo-input method [11], the disentanglement with pseudo-pairs preserves the details of the images and achieves much better accuracy and disentanglement. Besides, our method trains models end-to-end with much less computation.

## 2 Method

### 2.1 Notations and Preliminary

**Standard training.** Consider image classification with labeled training data $\mathcal{D}_{train} = \{(x, y)\}$, where $x \in \mathbb{R}^D$ is a $D$-dimensional input image, $y \in \{1, \dots, C\}$ denotes its class label, and $C$ is the number of classes. We can train a classifier $h$ with parameters $\theta$ by minimizing training loss as

$$\min_{\theta} \mathbb{E}_{(x,y)\sim\mathcal{D}_{train}} \mathcal{L}(\theta, x, y), \qquad \mathcal{L}(\theta, x, y) = l(h(x; \theta), y), \tag{1}$$

where $l(\cdot, \cdot)$ denotes the loss function, e.g. cross entropy, and $h(x; \theta)$ is the predicted probability distribution over $C$ classes. Assume the classifier has good standard accuracy after training.

**Adversarial example.** However, the standard classifier can be easily fooled by adversarial examples, generated with small perturbation $\delta$ to the input image that maximizes the loss function [26],

$$x^s_{adv} = x + \arg\max_{\delta \in \mathcal{S}} \mathcal{L}(\theta, x + \delta, y), \tag{2}$$

where $\mathcal{S} = \{\delta \mid \|\delta\|_p \leq \varepsilon\}$ is the set of all feasible perturbations within $\ell_p$ norm constraint. We refer to the classification accuracy under attack as robust accuracy.

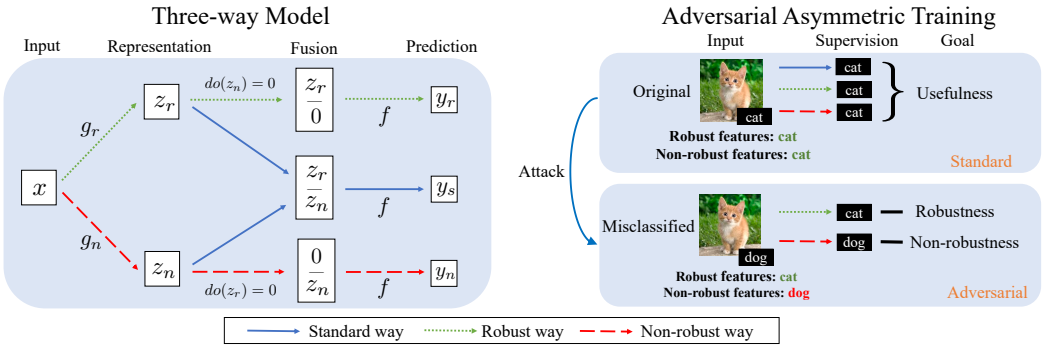



Figure 1: Left: a diagram of our proposed three-way model. We encode an input image $x$ into the robust and non-robust representations $z_r$ and $z_n$ with two encoders $g_r$ and $g_n$. Afterwards, we use three ways to combine the two representations and predict the labels with a shared classifier $f$. Right: an illustration of our proposed Adversarial Asymmetric Training with an image of a cat that is misclassified as a dog after adversarial perturbation. We assign asymmetric supervisions to the two representations to achieve robustness disentanglement.

**Adversarial training.** To alleviate adversarial attack, *Adversarial Training* (AT) [6] is proposed to train a robust classifier by solving the following robust optimization problem [17]

$$\min_{\theta} \mathbb{E}_{(x,y)\sim\mathcal{D}_{train}} \left[ \max_{\delta\in\mathcal{S}} \mathcal{L}(\theta, x+\delta, y) \right]. \tag{3}$$

Specifically, for a data sample $(x, y)$, we first solve the inner loop and get the adversarial example $x_{adv}$, and then update parameters $\theta$ with adversarial pair $(x_{adv}, y)$ for the outer loop.

**Robust and non-robust features.** Define a feature as a function mapping from the input space $\mathcal{X}$ to real numbers $h : \mathcal{X} \to \mathbb{R}$. With a specified data distribution $\mathcal{D}$ and an adversarial configuration $\mathcal{S}$, we give formal definitions of robust and non-robust features for binary classification ($C = 2$).

- We call a feature $h$ *$\rho$-useful* ($\rho > 0$) if it is correlated with the true label in expectation, i.e., $\mathbb{E}_{(x,y)\sim\mathcal{D}}[y \cdot h(x)] \geq \rho$.
- Suppose we have a $\rho$-useful feature $h$, we refer to $h$ as a *robust feature* (formally a $\gamma$-robustly useful feature) if $h$ remains $\gamma$-useful ($\gamma > 0$) under adversarial perturbation, i.e., $\mathbb{E}_{(x,y)\sim\mathcal{D}}\left[\min_{\delta\in\mathcal{S}} y \cdot h(x+\delta)\right] \geq \gamma$.
- We refer to $h$ as a *non-robust feature* (formally a $\gamma$-non-robustly useful feature) if it is $\rho$-useful for some $\rho > 0$, but not $\gamma$-robust ($\gamma > 0$).

In other words, both robust and non-robust features are useful for classification, and they differ merely in their behaviors under adversarial attack. As for their disentanglement, we should encourage both of them to attain better usefulness (higher $\rho$), while encourage robust features to attain better robustness (higher $\gamma$) and encourage non-robust features to attain better non-robustness (lower $\gamma$). We also give formal definitions for robust and non-robust representations likewise in Appendix A.1 and a discussion of the accuracy-robustness dilemma in Appendix A.2.

### 2.2 Model

We start by proposing a discriminative model for disentanglement. Given an input image $x$, we extract two representations through two encoders $g_r$ and $g_n$ with parameters $\theta_r$ and $\theta_n$,

$$\text{robust representation: } z_r = g_r(x; \theta_r); \tag{4a}$$
$$\text{non-robust representation: } z_n = g_n(x; \theta_n). \tag{4b}$$

and they are supposed to extract robust and non-robust features of the image, respectively, and thus disentangle them apart. Afterwards, the two representations are combined in three different ways and

get predictions with a shared classifier $f$ on the top,

$$\text{standard way: } h_s(x;\theta) = f([z_r, z_n]); \tag{5a}$$
$$\text{robust way: } h_r(x;\theta) = f([z_r, \mathbf{0}]); \tag{5b}$$
$$\text{non-robust way: } h_n(x;\theta) = f([\mathbf{0}, z_n]); \tag{5c}$$

where we denote $[\cdot,\cdot]$ for vector concatenation, and $\mathbf{0}$ for a zero vector of equal size as $z_r$ and $z_n$. See Figure 1 (left) for illustration. In $h_r$ and $h_n$, we set one of the representations to a constant vector to make it non-informative. From a causal view [31], essentially we are performing interventions [21] to eliminate the robust or non-robust features, i.e., $do(z_r) = 0$ or $do(z_n) = 0$.

### 2.3 Learning

In this part, we describe two training objectives for our model to achieve the disentanglement.

#### 2.3.1 Standard Training

By definition both robust and non-robust features are useful for prediction, thus all three ways should have high standard accuracy. Therefore, given a natural data pair $(x, y)$, we assign a standard classification loss to each of the three ways $h_s, h_r, h_n$, and get the standard training loss as

$$\mathcal{L}_{ST}(\theta, x, y) = l(h_s(x;\theta), y) + l(h_r(x;\theta), y) + l(h_n(x;\theta), y). \tag{6}$$

As a result, both representations are learned to be useful for prediction. Nevertheless, we can see that the supervisions for robust and non-robust representations are totally **symmetric** in the standard training loss. Therefore, the two representations cannot be disentangled at all.

#### 2.3.2 Adversarial Asymmetric Training

To further achieve disentanglement, we need to break this symmetry, and the key is nothing but adversarial examples. For a data pair $(x, y)$, we can generate an adversarial example $x^s_{adv}$ (Eq. 2) w.r.t. the standard way loss $l(h_s(x;\theta), y)$ to imitate attack to a standard classifier. We keep $x^s_{adv}$ if it is misclassified, i.e., its predicted class $\hat{y}_s \neq y$, and discard it otherwise. Because $x^s_{adv}$ is very close to $x$ (visually indistinguishable), by definition, its robust features are still about label $y$. In contrast, its non-robust features now belong to the misclassified class $\hat{y}_s$ due to the adversarial attack.

In this way we obtain an image with robust and non-robust features about different classes. This **asymmetry** enables us to disentangle the two representations with the following bi-level objective,

$$\begin{aligned} \mathcal{L}_{AS}(\theta, x, y) &= l(h_r(x^s_{adv};\theta), y) + l(h_n(x^s_{adv};\theta), \hat{y}_s), \\ \text{s.t. } &\begin{cases} x^s_{adv} = x + \underset{\delta\in\mathcal{S}}{\operatorname{argmax}}\ l(h_s(x+\delta;\theta), y), \\ \hat{y}_s = \operatorname{argmax}\ h_s(x^s_{adv};\theta),\ \hat{y}_s \neq y, \end{cases} \end{aligned} \tag{7}$$

where we let the robust way predict the original label $y$ from $z_r$ and let the non-robust way predict the perturbed label $\hat{y}_s$ from $z_n$. Therefore, the two asymmetric labels provide different supervisions to the two representations, such that $z_r$ stays invariant under attack (robust), and $z_n$ becomes sensitive to perturbations (non-robust). Therefore the two representations are disentangled.

The total loss is the combination of standard loss and adversarial loss for a balance between accuracy and disentanglement, and we re-organize it as

$$\begin{aligned} \mathcal{L}_{total}(\theta, x, y) &= \mathcal{L}_{ST}(\theta, x, y) + \mathcal{L}_{AS}(\theta, x, y) \\ &= l(h_s(x;\theta), y) + l(h_r(x;\theta), y) + l(h_r(x^s_{adv};\theta), y) \\ &\quad + l(h_n(x;\theta), y) + l(h_n(x^s_{adv};\theta), \hat{y}_s), \end{aligned} \tag{8}$$

where $(x^s_{adv}, \hat{y}_s)$ is generated according to Eq. 7. Overall, with the pseudo-pair $(x, x^s_{adv})$, we assign different goals to the three ways to learn robust and non-robust representations,

- **the standard way** $h_s$ should take both kinds of features to achieve better standard accuracy;
- **the robust way** $h_r$ is encouraged to be invariant to perturbations as it is supposed to predict label $y$ whether there is an adversary or not;

**Algorithm 1** A training episode loss computation of Adversarial Asymmetric Training (AAT)

**Input:** natural data pair $(x, y) \in \mathcal{D}_{train}$, current model parameters $\theta$;
**Output:** training loss $\mathcal{L}_{total}(\theta, x, y)$;

```
Predict x in three ways h_s, h_r, h_n (Eq. 5);
Calculate standard loss L_ST (Eq. 6);
Generate an adversarial example x^s_adv w.r.t. the standard way loss (Eq. 2);
if x^s_adv is misclassified then
    Predict x^s_adv in two ways h_r, h_n (Eq. 5);
    Calculate adversarial loss L_AS (Eq. 7);
    return loss L_total = L_ST + L_AS;
else
    return loss L_total = L_ST;
end if
```

- **the non-robust way** $h_n$ is taught to be very sensitive to input perturbations, as it predicts $x$ to original class $y$ and predicts $x^s_{adv}$, which is very close to $x$, to a different class $\hat{y}_s$.

To distinguish from Adversarial Training [6] that extracts robust features alone, we call our method *Adversarial Asymmetric Training* (AAT), which instead preserves both robust and non-robust features by disentanglement with asymmetric supervisions. See Figure 1 (right) for an example and Algorithm 1 for a complete description.

As we see, the pseudo-pairs are not given but a result of our training process. Remind that the prior of robustness is human-centric. Thus robustness comes from nowhere but our design of training objectives. In other words, the supervision of robustness is intrinsic rather than extrinsic. In our work, adversarial examples are not only "not bugs" [11], and they instead become the key to the disentanglement of robust and non-robust representations.

#### 2.3.3 AAT++

To further encourage the disentanglement of the two representations, we design two auxiliary asymmetric losses. In particular, to enhance the robustness of $z_r$, we perform robust optimization (Eq. 3) w.r.t. the robust way $h_r$, which can be written equivalently as

$$\mathcal{L}_{AR}(\theta, x, y) = l(h_r(x^r_{adv}; \theta),\ y), \quad \text{s.t. } x^r_{adv} = x + \underset{\delta \in \mathcal{S}}{\operatorname{argmax}}\ l(h_r(x+\delta;\theta), y). \tag{9}$$

Similarly, to enhance the non-robustness of $z_n$, we design the following objective for a non-robust-way adversarial example $x^n_{adv}$ misclassified as $\hat{y}_n$. As discussed above, the non-robust features of $x^n_{adv}$ belong to $\hat{y}_n$ due to adversarial attack. Therefore, we encourage the non-robust way $h_n$ to detect the non-robust features of $x^n_{adv}$ with supervision $\hat{y}_n$:

$$\mathcal{L}_{AN}(\theta, x, y) = l(h_n(x^n_{adv}; \theta), \hat{y}_n), \quad \text{s.t.} \begin{cases} x^n_{adv} = x + \underset{\delta \in \mathcal{S}}{\operatorname{argmax}}\ l(h_n(x+\delta;\theta), y), \\ \hat{y}_n = \operatorname{argmax}\ h_n(x^n_{adv}; \theta),\ \hat{y}_n \neq y. \end{cases} \tag{10}$$

The two auxiliary asymmetric losses here are designed to further "purify" each representation to be more robust or non-robust. Hence we coin the name AAT++ with total loss

$$\begin{aligned} \mathcal{L}^{++}_{total}(\theta, x, y) &= \mathcal{L}_{ST}(\theta, x, y) + \mathcal{L}_{AS}(\theta, x, y) + \mathcal{L}_{AR}(\theta, x, y) + \mathcal{L}_{AN}(\theta, x, y) \\ &= l(h_s(x;\theta), y) + l(h_r(x;\theta), y) + l(h_r(x^s_{adv};\theta), y) + l(h_r(x^r_{adv};\theta), y) \\ &\quad + l(h_n(x;\theta), y) + l(h_n(x^s_{adv};\theta), \hat{y}_s) + l(h_n(x^n_{adv};\theta), \hat{y}_n), \end{aligned} \tag{11}$$

where $(x^s_{adv}, \hat{y}_s), x^r_{adv}, (x^n_{adv}, \hat{y}_n)$ are generated according to Eq. 7, 9 & 10, respectively. As shown in our ablation study in Sec. 3.3, the auxiliary terms can enhance the robustness disentanglement in general, at the cost of sacrificing a little standard accuracy.

### 2.4 Adversarial Detection

Previous works have proposed various heuristics for detecting adversarial examples [29, 5, 19, 8, 2], yet typically without an understanding of the existence of adversarial examples. Our disentanglement of robust and non-robust features offers a principled approach for adversarial detection.

Table 1: WideResNet34 backbone results on CIFAR-10 (accuracy in percentage).

| Model | Method | Standard | | | Adversarial ($\ell_\infty$) | | | Adversarial ($\ell_2$) | | |
|---|---|---|---|---|---|---|---|---|---|---|
| | | S(↑) | R(↑) | N(↑) | R(↑) | N(↓) | DIA (↑) | R(↑) | N(↓) | DIA (↑) |
| 1-way | ST (baseline) | - | - | 95.1 | - | 0.0 | - | - | 33.8 | - |
| | AT [17] | - | 90.0 | - | **39.9** | - | - | **84.0** | - | - |
| | ST+AT | - | 90.0 | 95.1 | **39.9** | **0.0** | **39.9** | **84.0** | 33.8 | 50.2 |
| 3-way | PI [11] | 86.8 | 79.9 | 81.9 | 0.0 | **0.0** | 0.0 | 39.3 | **2.3** | 37.0 |
| | AAT (ours) | **95.2** | 91.1 | 94.7 | 21.7 | **0.0** | 21.7 | 81.7 | 25.0 | 56.7 |
| | AAT++ (ours) | 94.1 | 88.7 | 93.7 | **39.9** | **0.0** | **39.9** | 82.5 | 5.3 | **77.2** |

As discussed previously, the fundamental characteristic of (misclassified) adversarial examples is the disagreement between robust and non-robust features. Therefore, we can detect adversarial examples based on the two disentangled representations. Intuitively, if $z_r$ and $z_n$ agree, it is a natural image, otherwise it is adversarial. Here we give a simplest rule $D(x)$ to illustrate this idea,

$$y_r = \operatorname{argmax} h_r(x;\theta),\ y_n = \operatorname{argmax} h_n(x;\theta);\ \ D(x) = \begin{cases} 0 \text{ (natural)}, & \text{if } y_r = y_n; \\ 1 \text{ (adversarial)}, & \text{if } y_r \neq y_n, \end{cases} \tag{12}$$

that is, directly comparing the predictions from the two representations. This rule can be directly applied with our three-way model without extra computation. More complex strategies can also be considered to exploit more information from the disentangled representations, e.g. training an additional binary classifier [19] based on $z_r$ and $z_n$. We leave this for future work.

### 2.5 Evaluation Metric

Based on our model, we propose two evaluation metrics for robustness disentanglement. Similarly, the evaluation also does not require additional supervision on robustness.

**Difference in Accuracy (DIA).** For adversarial examples, the robust features are about the original label, while the non-robust features likely belong to a different class. This will lead to the high accuracy of the robust way and low accuracy of the non-robust way. In turn, a larger accuracy gap, namely *Difference in Accuracy*, indicates better disentanglement of the two representations.

**Rate of Adversarial Detection (RAD).** We devise a rule for adversarial detection in Sec. 2.4 by comparing inferred labels from robust and non-robust representations. Better disentanglement will yield a better detection rate, and in turn, a better detection rate also indicates better disentanglement.

## 3 Experiments

### 3.1 Setup

We conduct experiments on two well-known image classification tasks, MNIST and CIFAR-10. More experimental details can be found in Appendix B.

**Model.** We build our three-way model based on canonical CNNs for image classification. Specifically, we remove the output layer and take the remaining modules as an encoder. We use two such encoders as $g_r$ and $g_n$, and use a multi-layer perceptron on top as $f$. For CIFAR-10, we consider two backbones, WideResNet34 [30] and PreAct-ResNet18 [9]. For MNIST, we adapt from a small CNN [32]. The hyper-parameters are inherited from conventions [32] without any additional tuning.

**Evaluation.** In the test stage, we evaluate natural images via all three ways, denoted as S (standard), R (robust), N (non-robust). For white-box adversarial attack (see Table 4a for details), we evaluate the robust way with adversarial examples generated w.r.t. the robust-way loss, and likewise for the non-robust way. For completeness, we also include results for adversarial attack via the standard way, and our methods produce more promising results in this scenario. See Appendix C.

We also implement previous methods within our three-way model for a fair comparison. Note our implementations achieve comparable performance to the original work [27, 32].

- **One-way ST & AT.** Because the robust and non-robust ways utilize only one encoder and one representation, they are almost identical to a normal CNN classifier. Thus we use a

Table 2: PreAct-ResNet18 backbone results on CIFAR-10 (accuracy in percentage).

| Model | Method | Standard | | | Adversarial ($\ell_\infty$) | | | Adversarial ($\ell_2$) | | |
|---|---|---|---|---|---|---|---|---|---|---|
| | | S(↑) | R(↑) | N(↑) | R(↑) | N(↓) | DIA (↑) | R(↑) | N(↓) | DIA (↑) |
| 1-way | ST (baseline) | - | - | 94.2 | - | **0.0** | - | - | 35.1 | - |
| | AT [17] | - | 89.0 | - | **35.7** | - | - | **81.5** | - | - |
| | ST+AT | - | 89.0 | 94.2 | **35.7** | **0.0** | **35.7** | **81.5** | 35.1 | 46.4 |
| 3-way | PI [11] | 86.8 | 79.9 | 81.9 | 0.0 | 0.0 | 0.0 | 41.4 | **0.8** | 40.6 |
| | AAT (ours) | **94.8** | 91.8 | 93.8 | 10.8 | 0.0 | 10.8 | 79.9 | 22.1 | **57.8** |
| | AAT++ (ours) | 94.2 | 88.2 | 93.7 | 33.5 | **0.0** | 33.5 | 81.0 | 28.2 | 52.8 |

Table 3: MNIST classification results (accuracy in percentage).

| Model | Method | Standard | | | Adversarial ($\ell_2$) | | |
|---|---|---|---|---|---|---|---|
| | | S(↑) | R(↑) | N(↑) | R(↑) | N(↓) | DIA (↑) |
| 1-way | ST (baseline) | - | - | 99.5 | - | 17.9 | - |
| | AT [17] | - | 99.5 | - | **90.1** | - | - |
| | ST+AT | - | 99.5 | 99.5 | **90.1** | 17.9 | 72.2 |
| 3-way | AAT (ours) | **99.6** | 99.6 | 99.5 | 82.9 | 4.6 | 78.3 |
| | AAT++ (ours) | **99.6** | 99.5 | 99.4 | 89.9 | **0.0** | **89.9** |

single way of our model to implement traditional methods: Standard Training (ST) with the non-robust way $h_n$, and Adversarial Training (AT) [17] with the robust way $h_r$.[2]

- **ST+AT.** In fact, the simplest solution to extract robust and non-robust representations would be to combine a standard and robust classifier, though they may not be properly aligned. We can easily evaluate this method by combining the results of two separate models with one-way ST and AT as above.
- **PI (Pseudo-Input)** [11]. The authors offer robust and non-robust versions of CIFAR-10 as pseudo inputs.[3] We use them to learn disentangled representations in our three-way model. We train the robust way with the robust dataset and train the non-robust way with the non-robust datasets.

### 3.2 Classification Results

The quantitative results are illustrated in Table 1, 2 & 3. We mainly take WideResNet34 and $\ell_2$ attack in Table 1 for discussion and the rest are similar.

**Standard accuracy.** Comparing the standard accuracy of one-way ST and AT, we can see that adversarial training leads to a severe accuracy reduction ($\sim$5%) as it discards non-robust features. Instead, in our three-way model with AAT, the standard way effectively improves standard accuracy and is even competitive with standard training. AAT++ leads to a slight accuracy drop, but only by one percent. It shows our method successfully preserves standard accuracy by combining robust and non-robust features. However, another disentanglement approach, the pseudo-input method [11], leads to even worse standard accuracy (86.8%), indicating its iterative optimization over the input causes severe loss of details in the raw image.

**Adversarial accuracy and disentanglement.** The pseudo-input method indeed achieves some degree of disentanglement, which is, however, very limited (37.0% DIA), and diminishes quickly under stronger attack ($\ell_\infty$). In comparison, our pseudo-pair methods achieve much better disentanglement with better robust accuracy, 56.7% DIA of AAT and 77.2% DIA of AAT++. As for one-way methods, AT has the best robust accuracy (84.0%), yet the robust way of our AAT++ nearly matches this limit (82.5%) and is also competitive under stronger attack. Meanwhile, the non-robust way of AAT++ achieves much lower accuracy than one-way ST (5.3% v.s. 33.8%), indicating better non-robustness. Consequently, the disentanglement of our three-way model is better than the combination of two one-way models (77.2% v.s. 50.2% DIA). The advantage is more evident when the attack is relatively weak.

[2] We compare with half-half Adversarial Training [27] for a balance between standard and robust accuracy.

[3] `https://github.com/MadryLab/constructed-datasets`

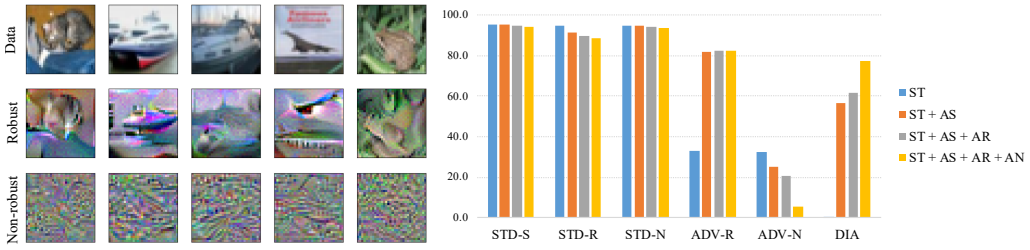
Table 4: (a) Configurations for adversarial attack, with range $\varepsilon$, $\ell_2$ or $\ell_\infty$ norm, step size $\alpha$, and $k$ steps of PGD [17]. (b) Adversarial detection and calibration results (accuracy in percentage). The model is evaluated on a equal mixture of natural and (standard-way) adversarial examples of CIFAR-10. RAD: rate of adversarial detection. Raw/Calibrated: classification accuracy before/after the calibration.

(a) Adversarial configurations.

| Data | Mode | Norm | $\varepsilon$ | $\alpha$ | $k$ |
|---|---|---|---|---|---|
| CIFAR-10 | Train | $\ell_\infty$ | 8/255 | 2/255 | 10 |
| | Test | $\ell_\infty$ | 8/255 | 2/255 | 20 |
| | | $\ell_2$ | 0.3 | 0.1 | 20 |
| MNIST | Train | $\ell_2$ | 0.3 | 0.01 | 5 |
| | Test | $\ell_2$ | 0.3 | 0.01 | 10 |

(b) Adversarial Detection.

| Method | RAD | Raw | Calibrated |
|---|---|---|---|
| PI [11] | 4.9 | 4.6 | 15.2 |
| AAT | 64.8 | 61.8 | 65.5 |
| AAT++ | **68.8** | **67.1** | **69.1** |




(a) Representation Inversion. (b) Ablation study.

Figure 2: (a) Visualization of robust and non-robust representations learned by AAT++. (b) Ablation study of the four losses of AAT++ (Eq. 11), with WideResNet34 backbone and $\ell_2$ attack on CIFAR-10. STD: standard. ADV: adversarial.

### 3.3 Further Analysis

**Ablation study.** We conduct ablation study for the four losses of AAT++ (Eq. 11), as shown in Figure 2b. $\mathcal{L}_{ST}$ achieves good standard accuracy but yields no disentanglement. The introduction of $\mathcal{L}_{AS}$ effectively achieves the disentanglement of two representations. Furthermore, adding $\mathcal{L}_{AR}$ improves the robust accuracy, and adding $\mathcal{L}_{AN}$ brings down the non-robust accuracy significantly. Combining four terms as in AAT++, we have the best disentanglement with the highest DIA score, while the standard accuracy drops a little in the meantime.

**Adversarial detection and calibration.** We evaluate our naïve detection rule (Eq. 12) and results are shown in Table 4b. The pseudo-input method performs much worse than random guess (4.9% RAD) because its robust accuracy is too poor. This also suggests its disentanglement is very limited. AAT and AAT++ instead enjoy considerably better detection rates. More complex strategies can be utilized for further improvement. As an additional application, we can also use the detection rule to calibrate our prediction for the mixture of natural and adversarial images. Specifically, we apply the robust way for inferred adversarial images and apply the standard way otherwise. From Table 4b, we can see that the calibration helps improve classification accuracy in total.

**Visualization.** To intuitively understand the disentanglement, we invert the two representations to input-level following [4]. From Figure 2a, we can see that the inversion of the robust representation is human-conceivable, while that of non-robust representation seems just plain noise. This is consistent with the phenomenon in previous work [4] that robust features are perceptually aligned with humans, while non-robust features are not. More qualitative results are included in Appendix D.

## 4 Related Work

Adversarial examples are proposed as a threat to machine learning models [26]. Afterwards, Adversarial Training [6] is developed to enhance robustness by feeding adversarial examples while training. Although effective, AT is found to be the cause of severe accuracy reduction, and the trade-off

between accuracy and robustness is fundamentally inevitable [27, 33]. Nevertheless, adversarial examples are not thus put to death and become useless. Recently, it is shown that it is possible to improve standard accuracy with adversarial examples [28]. Our work also contributes to this thread as we find adversarial examples can also serve as the fuel for disentangled representation learning.

Nevertheless, our method is not the only approach to utilize adversarial methods for disentanglement. AdvMix [7] instead disentangles "relevant" and "irrelevant" features w.r.t. class with a minimax game, while our work focuses on robustness disentanglement. However, AdvMix relies crucially on a pre-trained StyleGAN [12], while our method trains from scratch and is decoder-free.

In semi-supervised learning scenarios, previous works utilize virtual labels, i.e., the current inferred labels, to conduct adversarial training for unsupervised data [20, 24, 33]. In this work, we instead use virtual labels, $\hat{y}_s$ and $\hat{y}_n$, as supervisions for the non-robust features of adversarial examples. The virtual labels are found to work well as long as the current model is relatively precise.

## 5 Conclusion

In this paper, we have developed a novel Adversarial Asymmetric Training scheme for disentangling robust and non-robust representations without additional supervision on robustness. Our method is decoder-free, end-to-end, and achieves much better disentanglement compared to previous methods. Future work may include more efficient architecture designs, applications to other computer vision tasks, as well as advanced adversarial detection methods based on the disentangled representations.

## References


[1] Yoshua Bengio, Aaron Courville, and Pascal Vincent. Representation learning: A review and new perspectives. *IEEE transactions on pattern analysis and machine intelligence*, 35(8):1798–1828, 2013.

[2] Arjun Nitin Bhagoji, Daniel Cullina, and Prateek Mittal. Dimensionality reduction as a defense against evasion attacks on machine learning classifiers. *arXiv preprint arXiv:1704.02654*, 2, 2017.

[3] Anirban Chakraborty, Manaar Alam, Vishal Dey, Anupam Chattopadhyay, and Debdeep Mukhopadhyay. Adversarial attacks and defences: A survey. *arXiv preprint arXiv:1810.00069*, 2018.

[4] Logan Engstrom, Andrew Ilyas, Shibani Santurkar, Dimitris Tsipras, Brandon Tran, and Aleksander Madry. Learning perceptually-aligned representations via adversarial robustness. *arXiv preprint arXiv:1906.00945*, 2019.

[5] Zhitao Gong, Wenlu Wang, and Wei-Shinn Ku. Adversarial and clean data are not twins. *arXiv preprint arXiv:1704.04960*, 2017.

[6] Ian J Goodfellow, Jonathon Shlens, and Christian Szegedy. Explaining and harnessing adversarial examples. *arXiv preprint arXiv:1412.6572*, 2014.

[7] Sven Gowal, Chongli Qin, Po-Sen Huang, Taylan Cemgil, Krishnamurthy Dvijotham, Timothy Mann, and Pushmeet Kohli. Achieving robustness in the wild via adversarial mixing with disentangled representations. *arXiv preprint arXiv:1912.03192*, 2019.

[8] Kathrin Grosse, Praveen Manoharan, Nicolas Papernot, Michael Backes, and Patrick McDaniel. On the (statistical) detection of adversarial examples. *arXiv preprint arXiv:1702.06280*, 2017.

[9] Kaiming He, Xiangyu Zhang, Shaoqing Ren, and Jian Sun. Deep residual learning for image recognition. In *Proceedings of the IEEE conference on computer vision and pattern recognition*, pages 770–778, 2016.

[10] Irina Higgins, Loic Matthey, Arka Pal, Christopher Burgess, Xavier Glorot, Matthew Botvinick, Shakir Mohamed, and Alexander Lerchner. beta-vae: Learning basic visual concepts with a constrained variational framework. *ICLR*, 2(5):6, 2017.

[11] Andrew Ilyas, Shibani Santurkar, Dimitris Tsipras, Logan Engstrom, Brandon Tran, and Aleksander Madry. Adversarial examples are not bugs, they are features. *arXiv preprint arXiv:1905.02175*, 2019.

[12] Tero Karras, Samuli Laine, and Timo Aila. A style-based generator architecture for generative adversarial networks. In *Proceedings of the IEEE Conference on Computer Vision and Pattern Recognition*, pages 4401–4410, 2019.

[13] Hyunjik Kim and Andriy Mnih. Disentangling by factorising. *ICML*, 2018.

[14] Diederik P Kingma and Max Welling. Auto-encoding variational bayes. *NIPS*, 2014.

[15] Tejas D Kulkarni, William F Whitney, Pushmeet Kohli, and Josh Tenenbaum. Deep convolutional inverse graphics network. In *Advances in neural information processing systems*, pages 2539–2547, 2015.

[16] Francesco Locatello, Stefan Bauer, Mario Lucic, Gunnar Rätsch, Sylvain Gelly, Bernhard Schölkopf, and Olivier Bachem. Challenging common assumptions in the unsupervised learning of disentangled representations, 2018.

[17] Aleksander Madry, Aleksandar Makelov, Ludwig Schmidt, Dimitris Tsipras, and Adrian Vladu. Towards deep learning models resistant to adversarial attacks. In *International Conference on Learning Representations*, 2018.

[18] Michael F Mathieu, Junbo Jake Zhao, Junbo Zhao, Aditya Ramesh, Pablo Sprechmann, and Yann LeCun. Disentangling factors of variation in deep representation using adversarial training. In *Advances in Neural Information Processing Systems*, pages 5040–5048, 2016.

[19] Jan Hendrik Metzen, Tim Genewein, Volker Fischer, and Bastian Bischoff. On detecting adversarial perturbations. *ICLR*, 2017.

[20] Takeru Miyato, Shin-ichi Maeda, Masanori Koyama, and Shin Ishii. Virtual adversarial training: a regularization method for supervised and semi-supervised learning. *IEEE transactions on pattern analysis and machine intelligence*, 41(8):1979–1993, 2018.

[21] Judea Pearl. *Causality*. Cambridge university press, 2009.

[22] Ludwig Schmidt, Shibani Santurkar, Dimitris Tsipras, Kunal Talwar, and Aleksander Madry. Adversarially robust generalization requires more data. In *Advances in Neural Information Processing Systems*, pages 5014–5026, 2018.

[23] Narayanaswamy Siddharth, Brooks Paige, Jan-Willem Van de Meent, Alban Desmaison, Noah Goodman, Pushmeet Kohli, Frank Wood, and Philip Torr. Learning disentangled representations with semi-supervised deep generative models. In *Advances in Neural Information Processing Systems*, pages 5925–5935, 2017.

[24] Robert Stanforth, Alhussein Fawzi, Pushmeet Kohli, et al. Are labels required for improving adversarial robustness? *arXiv preprint arXiv:1905.13725*, 2019.

[25] Raphael Suter, Đorđe Miladinović, Bernhard Schölkopf, and Stefan Bauer. Robustly disentangled causal mechanisms: Validating deep representations for interventional robustness. *ICML*, 2019.

[26] Christian Szegedy, Wojciech Zaremba, Ilya Sutskever, Joan Bruna, Dumitru Erhan, Ian Goodfellow, and Rob Fergus. Intriguing properties of neural networks. *arXiv preprint arXiv:1312.6199*, 2013.

[27] Dimitris Tsipras, Shibani Santurkar, Logan Engstrom, Alexander Turner, and Aleksander Madry. Robustness may be at odds with accuracy. *arXiv preprint arXiv:1805.12152*, 2018.

[28] Cihang Xie, Mingxing Tan, Boqing Gong, Jiang Wang, Alan Yuille, and Quoc V Le. Adversarial examples improve image recognition. *arXiv preprint arXiv:1911.09665*, 2019.

[29] Weilin Xu, David Evans, and Yanjun Qi. Feature squeezing mitigates and detects carlini/wagner adversarial examples. *arXiv preprint arXiv:1705.10686*, 2017.

[30] Sergey Zagoruyko and Nikos Komodakis. Wide residual networks. *arXiv preprint arXiv:1605.07146*, 2016.

[31] Cheng Zhang, Kun Zhang, and Yingzhen Li. A causal view on robustness of neural networks. *arXiv preprint arXiv:2005.01095*, 2020.

[32] Dinghuai Zhang, Tianyuan Zhang, Yiping Lu, Zhanxing Zhu, and Bin Dong. You only propagate once: Painless adversarial training using maximal principle. *arXiv preprint arXiv:1905.00877*, 2019.

[33] Hongyang Zhang, Yaodong Yu, Jiantao Jiao, Eric P Xing, Laurent El Ghaoui, and Michael I Jordan. Theoretically principled trade-off between robustness and accuracy. *arXiv preprint arXiv:1901.08573*, 2019.

# A Additional Theoretical Discussions

## A.1 Definitions of Robust and Non-Robust Representations

Similar to the definitions of robust and non-robust features delivered in Sec. 2.1, here we present our definitions for robust and non-robust representations accordingly.

Define a representation $r$ as a function mapping from the input space $\mathcal{X}$ to a latent Space $\mathcal{Z}$ of lower dimension, $r : \mathcal{X} \to \mathcal{Z}$. We further define a classifier $f$ as a function mapping from the latent Space $\mathcal{Z}$ to real numbers, $f : \mathcal{Z} \to \mathbb{R}$. With a specified data distribution $\mathcal{D}$ and an adversarial configuration $\mathcal{S}$, we give formal definitions of robust and non-robust representations for binary classification ($C = 2$).

- We call a representation $r$ *$\rho$-useful* ($\rho > 0$) if there exists a classifier $f$, such that $h = f \circ r$ is correlated with the true label in expectation, i.e., $\mathbb{E}_{(x,y)\sim\mathcal{D}}[y \cdot h(x)] \geq \rho$.
- Suppose we have a $\rho$-useful representation $r$, we refer to $r$ as a *robust representation* (formally a $\gamma$-robustly useful representation) if, there exists a classifier $f$, such that $h = f \circ r$ remains $\gamma$-useful ($\gamma > 0$) under adversarial perturbation, i.e., $\mathbb{E}_{(x,y)\sim\mathcal{D}}\left[\min_{\delta\in\mathcal{S}} y \cdot h(x+\delta)\right] \geq \gamma$.
- We refer to $r$ as a *non-robust representation* (formally a $\gamma$-non-robustly useful representation) if it is $\rho$-useful for some $\rho > 0$, but not $\gamma$-robust ($\gamma > 0$).

## A.2 The Accuracy-Robustness Dilemma

As discussed in the main text, there is a fundamental trade-off between accuracy and robustness that enhancing robustness will inevitably lead to the degradation of standard accuracy. Besides the empirical evidence given in previous work [27], it is shown that the accuracy-robustness dilemma exits even if we have infinite data and optimal classifiers. Here, we present such an example to illustrate the phenomenon. Our example is a variation of the one presented in [27], which we review as follows.

**The binary classification problem in [27].** The data model consists of input-label pairs $(x, y)$ sampled from a distribution $\mathcal{D}$ as follows:

$$y \sim \overset{u.a.r}{\{-1,+1\}}, \quad x_1 = \begin{cases} +y, & \text{w.p. } p \\ -y, & \text{w.p. } 1-p' \end{cases} \quad x_2, \ldots, x_{d+1} \overset{i.i.d}{\sim} \mathcal{N}(\eta y, 1) \tag{13}$$

For this problem, a natural classifier

$$f_{\text{avg}}(x) := \text{sign}\left(w_{\text{unif}}^\top x\right), \quad \text{where } w_{\text{unif}} := \left[0, \frac{1}{d}, \ldots, \frac{1}{d}\right] \tag{14}$$

achieves standard accuracy arbitrarily close to $100\%$, for $d$ large enough. However, an $\ell_\infty$-bounded adversary with $\varepsilon = 2\eta$, can shift the weakly-correlated features $\{x_2, \ldots, x_{d+1}\}$ towards $-y$. As a result, the simple classifier that relies solely on these non-robust features cannot get adversarial accuracy better than $1\%$.

On the contrary, assume $p > 0.5$, the classifier relying solely on robust features

$$f_{rob}(x) = \text{sign}\left(w_{rob}^\top x\right), \quad \text{where } w_{rob} := [1, 0, \ldots, 0] \tag{15}$$

will have $p$ accuracy in expectation under both standard and adversarial scenarios. $f_{rob}$ attains better robustness, at the cost of sacrificing accuracy ($p < 1$). Such a trade-off between accuracy and robustness is fundamental and will not disappear even with infinite samples and Bayes-optimal classifiers.

**Limitations.** The example above gives a clear illustration of the dilemma. However, the problem setup is somewhat misleading because it suggests that a classifier relying solely on non-robust features can achieve optimal accuracy. In fact, as shown in our experiments, such a classifier usually has

sub-optimal standard accuracy, similar to the robust classifier. Only the standard way that combines robust and non-robust features can achieve comparable performance to the one-way ST model. Here, we give a variation of their example that shows not only the accuracy-robustness dilemma but also the benefit of preserving both robust and non-robust features.

**Our example.** We consider the case where input pair $(x, y)$ follows distribution

$$y \overset{u,a,r}{\sim} \{-1, +1\}, x_i = \begin{cases} +\eta_i y, & \text{w.p. } p \\ -\eta_i y, & \text{w.p. } 1-p \end{cases}, \ i \in [d]. \tag{16}$$

For simplicity we assume $p = 0.8, d = 7$, and

$$\eta_1 = \eta_2 = \eta_3 = \eta_4 = 0.01, \ \eta_5 = \eta_6 = \eta_7 = 1.$$

**Proposition 1.** *For the problem above, we have the following conclusions:*

*1) The following linear classifier*

$$h_0(x) := \text{sign}\left(w_0^\top x\right), w_0 = \left[\frac{1}{\eta_1}, \frac{1}{\eta_2}, \ldots, \frac{1}{\eta_7}\right]^\top. \tag{17}$$

*has $94.4\%$ standard accuracy in expectation and it is Bayes-optimal. Nevertheless, it always has 0% accuracy under $\ell_\infty$ attack with $\varepsilon = 0.02$, because the adversary can shift the non-robust features $[x_1, x_2, x_3, x_4]$, towards $-y$.*

*2) Instead, the classifier*

$$h_1(x) := \text{sign}\left(w_1^\top x\right), w_1 = \left[0, 0, 0, 0, \frac{1}{\eta_5}, \frac{1}{\eta_6}, \frac{1}{\eta_7}\right]^\top. \tag{18}$$

*is optimal under attack, because it relies solely on the last three robust features $[x_5, x_6, x_7]$. $h_1$ attains 88.0% accuracy in expectation for both standard and adversarial scenarios.*

**Discussion.** In our problem setup, neither robust nor non-robust features are perfect. Each of them can be misleading for the correct label with a certain probability, and their combination can average out the risks and yield optimal standard accuracy, which is more consistent with our experimental results discussed in Sec. 3. It also suggests that standard training that aims at best accuracy is not enough to extract solely non-robust features. Instead, besides the usefulness pursued by standard training, our AAT and AAT++ further enhance the non-robustness of our non-robust way by enforcing it to be sensitive to adversarial perturbations.

*Proof.* 1) For simplicity, we denote $\hat{x}_i = x_i/\eta_i$ for re-weighted features. Then the linear classifier

$$h_0(x) = \text{sign}\left(\sum_{i=1}^{7} \hat{x}_i\right), \quad \hat{x}_i \in \{\pm 1\},$$

is equivalent to a majority voting method, and its classification is wrong only when there are at least four $x_i$'s indicating $-y$. Hence the expected standard accuracy of $h_0$ follows

$$P\left(h_0(x) = y\right) = 1 - C_7^4(1-p)^4 = 1 - 35 \times 0.0016 = 0.944. \tag{19}$$

Next, we prove its optimality. According to the problem setup, we have

$$P(Y = y|X = x) = \frac{P(X = x|Y = y)P(Y = y)}{P(X = x)} = \prod_i \frac{p^{(\hat{x}_i y+1)/2}(1-p)^{(1-\hat{x}_i y)/2}}{\sum_y p^{(\hat{x}_i y+1)/2}(1-p)^{(1-\hat{x}_i y)/2}}. \tag{20}$$

And the decision rule of the Bayes-optimal classifier should be

$$h^*(x) = \begin{cases} +1, & \text{if } P(Y = y|X = x) \geq \frac{1}{2}; \\ -1, & \text{otherwise.} \end{cases} \tag{21}$$

Notice that if there are 4 $\hat{x}_i$'s different from $y$, we have

$$P(Y = y|X = x) = \frac{p^3(1-p)^4}{p^3(1-p)^4 + p^4(1-p)^3} \approx 0.2 < 0.5, \tag{22}$$

and the probability is smaller with more such features. So the Bayes-optimal classifier is right when they are at most 3 $\hat{x}_i$'s different from $y$. Following Eq. 19, we can conclude that the expected standard accuracy of the Bayes-optimal classifier could be no more than $0.944$. Because $h_0$ achieves this expected accuracy, it is optimal.

2) Because the specified adversary can change the sign of non-robust features arbitrarily, the first four features $[x_1, x_2, x_3, x_4]$ becomes non-informative. Hence we can only rely on the robust features $[x_5, x_6, x_7]$. Following the same deduction in Eq. 19, $h_1$'s expected robust accuracy is

$$P\left(h_1(x) = y\right) = 1 - C_3^2(1-p)^2 = 1 - 3 \times 0.04 = 0.88. \tag{23}$$

In fact, it is optimal under adversarial attack. It is easy to tell that $h_1$'s expected standard accuracy of is also 88%. Compared to $h_0$, it becomes much more robust, but at the cost of sacrificing $6.4\%$ standard accuracy. $h_0$ can achieve the best standard accuracy because it preserves both robust and non-robust features in the input. It shows that the trade-off between accuracy and robustness occurs even with infinite data and Bayes-optimal classifiers. □

# B Additional Experimental Setup

## B.1 Model

In our three-way model, the two encoders, $g_r$ and $g_n$, are beheaded classification models with the same architecture. Hence they provide two representations of the same size $H$. As for the shared classifier on top, the first linear layer has a size of $2H \times H$, followed by a ReLU activation and another linear layer of the size $H \times C$, where $C$ is the number of classes.

## B.2 Training

We list our training configurations in Table 5. All these hyper-parameters are directly immigrated from the YOPO repository, see `https://github.com/a1600012888/YOPO-You-Only-Propagate-Once`. We implement our methods with PyTorch and conduct experiments on NVIDIA P100 GPUs.

Table 5: Training Configurations in our experiments.

| Task | Backbone | Learning Rate | Momentum | Weight Decay | Epoch | Milestones |
|---|---|---|---|---|---|---|
| CIFAR-10 | Wide34 | 0.1 | 0.9 | 2e-4 | 105 | [75, 90,100] |
| | Res18 | 0.05 | 0.9 | 5e-4 | 105 | [75, 90,100] |
| MNIST | CNN | 0.1 | 0.9 | 5e-4 | 56 | [50,55] |

# C Additional Quantitative Results

In Sec. 3, we show adversarial accuracies obtained under attack w.r.t. the robust and non-robust way loss, respectively. In this part, we include additional results when the attack is crafted w.r.t. the standard way of our model, which resembles the attack to a standard classifier.

From Table 6, 7, 8, we can see AAT can yield even better robust accuracy than one-way AT under standard-way attack, and AAT++ can generally achieve better robustness. The disentanglement score is also better than the pseudo-input method.

Nevertheless, we notice that our non-robust accuracy is not as good as the pseudo-input method. Meanwhile, its non-robust-way standard accuracy is much lower than ours, due to the loss of details in the raw image. It indicates that the combination of the pseudo-input and pseudo-pair methods might produce better disentanglement without loss of accuracy. We leave this for future work.

# D Additional Qualitative Results

Here, in Figure 3 & 4, we give more qualitative results to show the difference between two disentangled representations, including the gradient visualization task [27] and the representation inversion

Table 6: CIFAR-10 results (accuracy in percentage) with WideResNet34 backbone with attack w.r.t. the standard way.

| Model | Training | Adversarial ($\ell_\infty$) | | | | Adversarial ($\ell_2$) | | | |
|---|---|---|---|---|---|---|---|---|---|
| | | S(-) | R(↑) | N(↓) | DIA (↑) | S(-) | R(↑) | N(↓) | DIA (↑) |
| 1-way | ST | - | - | 0.0 | - | - | - | 33.8 | - |
| | AT [17] | - | 39.9 | - | - | - | 84.0 | - | - |
| 3-way | PI [11] | 0.0 | 5.2 | 0.0 | 5.2 | 22.5 | 64.8 | **4.9** | 59.9 |
| | AAT (ours) | 0.0 | 59.5 | 0.0 | 59.5 | 69.0 | 89.8 | 35.2 | 54.6 |
| | AAT++ (ours) | 9.8 | **66.4** | 0.0 | **66.4** | 77.9 | **89.0** | 23.7 | **65.3** |

Table 7: CIFAR-10 results (accuracy in percentage) with Pre-activated ResNet18 backbone with attack w.r.t. the standard way.

| Model | Training | Adversarial ($\ell_\infty$) | | | | Adversarial ($\ell_2$) | | | |
|---|---|---|---|---|---|---|---|---|---|
| | | S(-) | R(↑) | N(↓) | DIA (↑) | S(-) | R(↑) | N(↓) | DIA (↑) |
| 1-way | ST | - | - | 0.0 | - | - | - | 35.1 | - |
| | AT [17] | - | 35.7 | - | - | - | 81.5 | - | - |
| 3-way | PI [11] | 0.0 | 8.2 | 0.0 | 8.2 | 21.6 | 65.7 | **1.3** | **64.4** |
| | AAT (ours) | 0.2 | 38.9 | 0.0 | 38.9 | 66.6 | 88.1 | 31.4 | 56.7 |
| | AAT++ (ours) | 1.3 | **63.8** | 0.0 | **63.8** | 68.4 | **86.5** | 35.3 | 51.2 |

task [4]. They both show that the robust representations are perceptually aligned with humans while the non-robust representations seem plain noise. Details of implementation are as follows.

### D.1 Gradient Visualization

We show the gradient for a clean image w.r.t. the robust and non-robust way loss as in [27]. For each image pair $(x, y)$ and the specified classifier $h$, we calculate the gradient w.r.t. the input $\nabla_x \, l(h(x;\theta), y)$. We clip gradients to $\pm 3$ standard deviations of their mean and rescale them to the range $[0, 1]$.

### D.2 Representation Inversion

Following [4], we inverse each representation to input and see what we can get. We initialize the input from random noise and optimize it by minimizing the distance between its robust (or non-robust) representation and the target representation, similar to the construction of robust and non-robust datasets in [11]. We use a learning rate of 1.0 with 10000 steps for CIFAR-10.

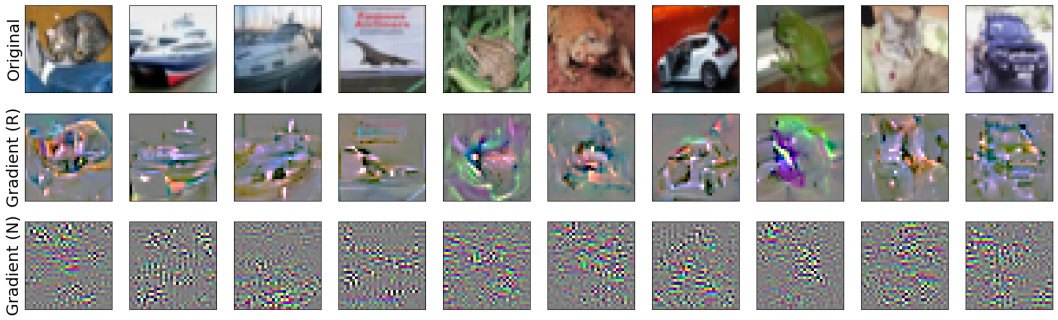



Figure 3: Gradient visualization with WideResNet34 backbone on CIFAR-10.

Table 8: MNIST results (accuracy in percentage) with attack w.r.t. the standard way.

| Model | Training | Adversarial ($\ell_2$) | | | |
|---|---|---|---|---|---|
| | | S(-) | R(↑) | N(↓) | DIA (↑) |
| 1-way | ST | - | - | 17.4 | - |
| | AT [17] | - | 89.8 | - | - |
| 3-way | AAT (ours) | 51.0 | 93.9 | 30.4 | 63.5 |
| | AAT++ (ours) | 12.6 | 97.8 | 7.3 | 90.5 |

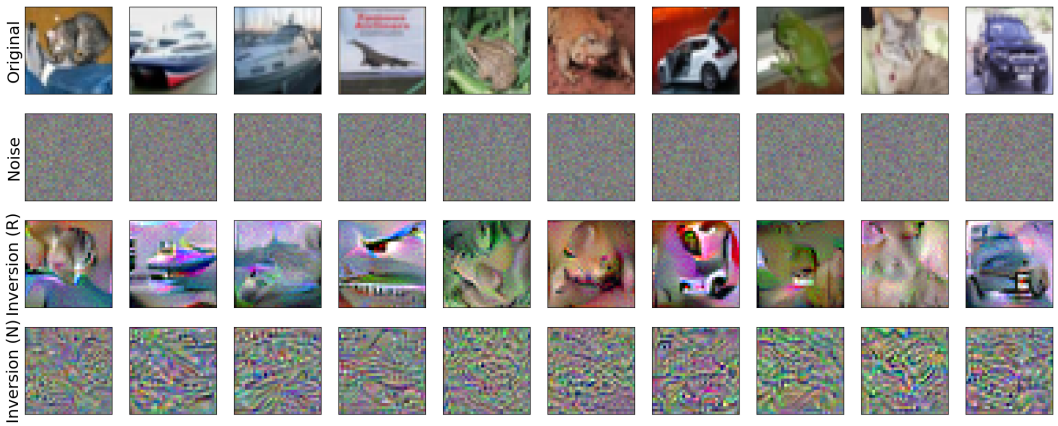



Figure 4: Representation inversion with WideResNet34 backbone on CIFAR-10.